Positional and Orientational Disorder in a Solid Solution of $Sr_{9+x}Ni_{1.5-x}(PO_4)_7$ ($x = 0.3$)

A. A. Belik,[†,‡] F. Izumi,*[,†] T. Ikeda,[†] V. A. Morozov,[§] R. A. Dilanian,[†] S. Torii,[∥] E. M. Kopnin,[†] O. I. Lebedev,[§] G. Van Tendeloo,[§] and B. I. Lazoryak[⊥]

Advanced Materials Laboratory, National Institute for Materials Science, 1-1 Namiki, Tsukuba, Ibaraki 305-0044, Japan, Department of Chemistry, Moscow State University, Leninsky Gory, Moscow 119899, Russia, Electron Microscopy for Materials Research, University of Antwerp, Groenenborgerlaan 171, B-2020 Antwerp, Belgium, and Institute of Materials Science, University of Tsukuba, 1-1-1 Ten-nodai, Tsukuba, Ibaraki 305-8573, Japan

Received June 25, 2002. Revised Manuscript Received August 14, 2002

Solid solutions of $Sr_{9+x}Ni_{1.5-x}(PO_4)_7$ that are structurally related to β-$Ca_3(PO_4)_2$ are formed in the compositional range of $0.14 \leq x \leq 0.39$. We investigated static disorder in $Sr_{9.3}Ni_{1.2}(PO_4)_7$ ($x = 0.3$, space group: $R\bar{3}m$) by X-ray and neutron powder diffraction. The electron-density distribution in $Sr_{9.3}Ni_{1.2}(PO_4)_7$ was determined by Rietveld refinement and subsequent whole-pattern fitting based on the maximum entropy method (MEM) from synchrotron X-ray powder diffraction data measured at 100 K. The resulting electron densities served to derive an expedient split-atom model. By adopting this model, we refined the structure parameters of $Sr_{9.3}Ni_{1.2}(PO_4)_7$ by the Rietveld method from the X-ray diffraction data as well as from time-of-flight neutron powder diffraction data measured at 293 K. The Rietveld refinement with the X-ray diffraction data gave $R_{wp} = 5.39\%$ and $R_B = 2.80\%$. Further MEM-based pattern fitting appreciably decreased the R factors to $R_{wp} = 5.18\%$ and $R_B = 1.03\%$, which demonstrates that the highly disordered structure of $Sr_{9.3}Ni_{1.2}(PO_4)_7$ can be expressed more accurately with electron densities than with structure parameters. The asymmetric unit of $Sr_{9.3}Ni_{1.2}(PO_4)_7$ contains two Sr sites (Sr1 and Sr3), one Ni site (Ni5), one mixed-metal site (M4), two P sites (P1 and P2), and five O sites. Sr3 atoms are statistically distributed among four positions near the center of symmetry. Sr^{2+} and Ni^{2+} ions are split to occupy the M4 site that is 75% vacant. $P1O_4$ tetrahedra are orientationally disordered.

1. Introduction

During the past decade, the maximum entropy method (MEM) has been applied to the visualization of the electron-density distribution from X-ray powder diffraction (XRD) data.[1] Takata et al.[1] developed the so-called MEM/Rietveld method (Figure 1). This method consists of Rietveld refinement[2] followed by MEM analysis. "Observed" structure factors, F_o(Rietveld), estimated from the structure, profile, and other parameters refined in Rietveld analysis[2] are analyzed by MEM to give electron densities in the unit cell. The electron-density distribution is visualized and carefully examined to modify the structural model in the Rietveld analysis when necessary. Rietveld refinements and MEM analyses are repeated until crystal data obtained by the former are judged to be consistent with electron densities determined by the latter.

Unfortunately, F_o(Rietveld) data are biased toward the structural model of Rietveld analysis because both the phases and integrated intensities utilized to partition the observed diffraction intensities are calculated from final structure parameters.[3] This bias, more or less, lowers the accuracy of the electron densities derived by the MEM/Rietveld method.

To overcome the defect of the MEM/Rietveld method, Izumi et al.[4] devised sophisticated methodology for structure refinement: MEM-based pattern fitting (MPF). In MPF, the bias toward the structural model is reduced as much as possible by an iterative procedure outlined in Figure 1. Structure factors, F_c(MEM), are calculated by the Fourier transform of electron densities resulting from MEM analysis. Next, we proceed to whole-pattern fitting where only the parameters that are irrelevant to the crystal structure are refined with structure factors fixed at F_c(MEM). Observed structure factors, F_o(MPF), estimated after the pattern fitting by Rietveld's procedure[2] are analyzed again by MEM. In such a manner, MEM analyses and whole-pattern fitting are alternately repeated (REMEDY cycles) until R factors

* Corresponding author. E-mail: IZUMI.Fujio@nims.go.jp. Tel: +81 (298) 51-3354 (ext. 511). Fax: +81 (298) 52-7449.
[†] National Institute for Materials Science.
[‡] Postdoctoral fellow from the Department of Chemistry, Moscow State University, Leninsky Gory, Moscow 119899, Russia.
[§] University of Antwerp.
[∥] University of Tsukuba.
[⊥] Moscow State University.

(1) Takata, M.; Nishibori, E.; Sakata, M. *Z. Kristallogr.* **2001**, *216*, 71.
(2) Rietveld, H. M. *J. Appl. Crystallogr.* **1969**, *2*, 65.
(3) McCusker, L. B.; Von Dreele, R. B.; Cox, D. E.; Louër, D.; Scardi, P. *J. Appl. Crystallogr.* **1999**, *32*, 36.
(4) Izumi, F.; Kumazawa, S.; Ikeda, T.; Hu, W.-Z.; Yamamoto, A.; Oikawa, K. *Mater. Sci. Forum* **2001**, *378*−*381*, 59.

10.1021/cm0206901 CCC: $22.00
Published on Web 10/03/2002

no longer decrease. Observed diffraction intensities to which two or more Bragg reflections contribute are repartitioned more appropriately with an increasing number of REMEDY cycles, which stems from the extraction of additional structural information from the observed diffraction intensities by MEM. In addition, structure factors, F_o, that are observed actually can be determined for isolated reflections without any approximations. Thus, the structural model affects the F_o(MPF) data to a lesser extent with increasing iterations of MPF. The MPF method is also applicable to the determination of scattering-length (nuclear) densities from neutron powder diffraction data.

In the MPF method, crystal structures are expressed not by structure parameters such as fractional coordinates and atomic displacement parameters but by electron densities in the unit cell. Hence, MPF permits a more adequate representation of disordered atomic configurations, chemical bonding, nonlocalized electrons, and anharmonic thermal motion than conventional Rietveld analysis. Pair distribution-function analysis of neutron or X-ray powder diffraction data is a useful technique for obtaining local nonrandom atomic displacements in both amorphous and crystalline materials.[5] On the other hand, the MPF method is effective in the analysis of average structures for crystalline materials showing static and dynamic disorder. This original technique of structure refinement has successfully been applied to several inorganic materials: the positional disorder of K^+ ions interlayered in $K_xTi_{2-x/3}Li_{x/3}O_4$,[4,6] atomic arrangements of K clusters in a K-type zeolite Linde Type A,[7] the nuclear/electron-density distribution in a high-T_c superconductor $HgBa_2CuO_{4+\delta}$,[4,8] the ab initio structure analysis of a helix-layered silicate,[9] and conduction pathways in a high ionic conductor $Rb_4Cu_{16}I_{7.2}Cl_{12.8}$.[10]

Belik et al.[11−13] have recently reported that strontium phosphates $Sr_{9+x}M_{1.5-x}(PO_4)_7$ (M = Mn, Fe, Co, Ni, Cu, and Cd) that are structurally similar to β-$Ca_3(PO_4)_2$ contain highly disordered atoms. Structure parameters of $Sr_9Fe_{1.5}(PO_4)_7$[12] and $Sr_{9.1}Cu_{1.4}(PO_4)_7$[13] were refined from XRD data by using space group $R\bar{3}m$ ($a \approx 10.6$ Å and $c \approx 19.7$ Å). However, details in the disordered configurations of part of the Sr^{2+}, M^{2+}, and PO_4^{3-} ions in the two phosphates remain obscure on account of difficulty in building reasonable split-atom models; their structures need further investigation. Phosphates with nominal compositions of $A_{9.333}Ni_{1.167}(PO_4)_7$ (A = Ca and Sr) are commercial catalysts for dehydrogenation (e.g., for converting 1- and 2-butenes to butadience and for oxydehydrogenating lower aliphatic alkanes and alkenes to dienes).[14] XRD suggested that $Ca_{9.333}Ni_{1.167}(PO_4)_7$ bears a close structural resemblance to $Sr_{9+x}Ni_{1.5-x}(PO_4)_7$. $Sr_{9+x}M_{1.5-x}(PO_4)_7$:$Sn^{2+}$ (M = Mg, Zn, and Cd) were studied in expectation of their applications as luminescent materials.[15] We should provide insight into structure−property relationships in these systems with reference to reliable structural knowledge including static disorder and distribution of metals.

In the present work, we have prepared solid solutions with nominal compositions of $Sr_{9+x}Ni_{1.5-x}(PO_4)_7$ ($0 \le x \le 0.5$), characterized them by some physical methods, and elucidated the crystal structure of $Sr_{9.3}Ni_{1.2}(PO_4)_7$ ($x = 0.3$) from its synchrotron X-ray and time-of-flight (TOF) neutron powder diffraction data. Our analysis of synchrotron XRD by MPF has made it possible to rebuild a split-atom model for Rietveld analysis, visualize the electron-density distribution in $Sr_{9.3}Ni_{1.2}(PO_4)_7$, and furnish a significant amount of information as to its structural properties pertaining to positional and orientational disorder. The MPF method is more suitable for representing the orientational disorder of phosphate ions in the present compound than the spherical harmonics approach because of the rather uneven distribution of four oxygen atoms around each P atom.

2. Experimental Section

Synthesis. Solid solutions with nominal compositions of $Sr_{9+x}Ni_{1.5-x}(PO_4)_7$ ($x = 0$, 0.1, 0.15, 0.2, 0.25, 0.3, 0.35, 0.4, 0.45, and 0.5) were synthesized by the solid-state method from mixtures of $SrCO_3$ (99.999%), NiO (99.0%), and $NH_4H_2PO_4$ (99.999%). The mixtures were placed in alumina crucibles, heated in air while raising the temperature very slowly from room temperature (RT) to 870 K, and then kept at 1300 K for 120 h with three intermediate grindings. The products were quenched to RT. They were light pink.

XRD Experiments with Characteristic X-rays. XRD data of the products were measured at RT on a SIEMENS D500 Bragg−Brentano-type powder diffractometer operated at 30 kV and 30 mA. The diffractometer was equipped with an incident-beam quartz monochromator to take out Cu $K\alpha_1$ radiation ($\lambda = 1.5406$ Å) and a BRAUN position-sensitive detector. Si (NIST standard reference material 640b) was used as an external standard material for diffraction angles. For phase identification, XRD data were collected in a 2θ range from 10 to 80° with a step interval of 0.02°. The resultant XRD data were analyzed by the Rietveld method[2] with RIETAN-2000.[16] We refined only the scale factors and lattice parameters of $Sr_{9+x}Ni_{1.5-x}(PO_4)_7$ and impurities (i.e., $Sr_3(PO_4)_2$[17] and $Sr_2Ni(PO_4)_2$[18]), fixing their structure parameters at those reported in the literature. Mass fractions of constituent phases were evaluated from the refined scale factors.

Synchrotron XRD Experiments and Structure Refinements by Rietveld Analysis and MPF. Synchrotron XRD

(5) Toby, B. H.; Egami, T. *Acta Crystallogr., Sect. A* **1992**, *48*, 336.
(6) Izumi, F.; Ikeda, T.; Sasaki, T.; Kumazawa, S. *Mol. Cryst. Liq. Cryst.* **2000**, *341*, 1057.
(7) Ikeda, T.; Kodaira, T.; Izumi, F.; Kumazawa, S. *Mol. Cryst. Liq. Cryst.* **2000**, *341*, 1251.
(8) Izumi, F.; Yamamoto, A.; Khasanova, N. R.; Kumazawa, S.; Hu, W.-Z.; Kamiyama, T. *Physica C* **2000**, *335*, 239.
(9) Ikeda, T.; Akiyama, Y.; Izumi, F.; Kiyozumi, Y.; Mizukami, F.; Kodaira, T. *Chem. Mater.* **2001**, *13*, 1286.
(10) Oikawa, K.; Kamiyama, T.; Kanno, R.; Izumi, F.; Ikeda, T.; Chakoumakos, B. C. *Mater. Sci. Forum*, in press.
(11) Belik, A. A.; Izumi, F.; Ikeda, T.; Lazoryak, B. I.; Morozov, V. A.; Malakho, A. P.; Stefanovich, S. Yu.; Grebenev, V. V.; Shelmenkova, O. V.; Kamiyama, T.; Oikawa, K.; Leonidov, I. A.; Leonidova, O. N.; Davydov, S. A. *Phosphorus, Sulfur, Silicon Relat. Elem.* **2002**, *177*, 1899.
(12) Belik, A. A.; Lazoryak, B. I.; Pokholok, K. V.; Terekhina, T. P.; Leonidov, I. A.; Mitberg, E. B.; Karelina, V. V.; Kellerman, D. G. *J. Solid State Chem.* **2001**, *162*, 113.
(13) Belik, A. A.; Malakho, A. P.; Lazoryak, B. I.; Khasanov, S. S. *J. Solid State Chem.* **2002**, *163*, 121.
(14) (a) The Dow Chemical Co. U.S. Patent 3,935,126, 1974. (b) General Electric Co. U.S. Patent 4,346,249, 1981. (c) General Electric Co. U.S. Patent 4,366,089,1981. (d) The Dow Chemical Co. U.S. Patent 4,471,146, 1983. (e) Lee, S. J.; Jun, J. H.; Lee, S.-H.; Yoon, K. J.; Lim, T. H.; Nam, S.-W.; Hong, S.-A. *Appl. Catal., A* **2002**, *230*, 61.
(15) Donker, H.; Smit, W. M. A.; Blasse, G. *J. Electrochem. Soc.* **1989**, *136*, 3130.
(16) Izumi, F.; Ikeda, T. *Mater. Sci. Forum* **2000**, *321−324*, 198.
(17) Sugiyama, K.; Tokonami, M. *Mineral. J.* **1990**, *15*, 141.
(18) Elbali, B.; Boukhari, A. *Acta Crystallogr., Sect. C* **1993**, *49*, 1131.

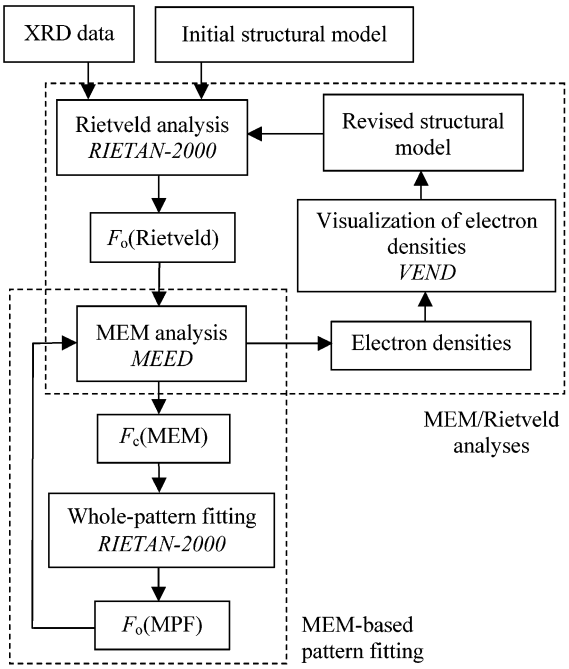

Figure 1. Structure refinement by Rietveld and MEM analyses followed by iterative whole-pattern fitting based on MEM.

data of $Sr_{9.3}Ni_{1.2}(PO_4)_7$ were measured at 100 K on a powder diffractometer (BL15XU at SPring-8) with Debye−Scherrer geometry using a Ge(111) analyzer. Incident beams from an undulator were monochromatized to a wavelength of 0.8000 Å with rotated inclined Si(111) double-crystal monochromators. The sample was loaded into a quartz-glass capillary tube with an inner diameter of 0.3 mm and was rotated at a speed of 6.3 rad/s. The μr (μ: linear absorption coefficient, r: sample radius) value of the sample plus the capillary tube was determined by measuring the transmittance of the direct incident beam to correct for the absorption of X-rays. The XRD data were collected in a 2θ range from 5.2 to 90.1° with a step interval of 0.003° and a counting time of 1 s/step.

Structure parameters of $Sr_{9.3}Ni_{1.2}(PO_4)_7$ were refined by the Rietveld method from the synchrotron XRD data using RIETAN-2000.[16] The split pseudo-Voigt function of Toraya[19] was used as a profile function. The background was represented by a composite background function (i.e., an 11th-order Legendre polynomial multiplied by a set of numerical values obtained with PowderX[20] to approximate the background). Coefficients for the analytical approximation to atomic scattering factors for Sr, Ni, P, and O were taken from ref 21. Anomalous scattering factors were evaluated with CROMER by the Cromer−Liberman method adopting a Kissel−Pratt correction.[22] Isotropic atomic-displacement parameters, U, with the isotropic Debye−Waller factor formulated as $\exp(-8\pi^2 U \sin^2\theta/\lambda^2)$ were assigned to all the sites.

In MPF, we used XRD data in a 2θ range from 5.2 to 48° corresponding to $d > 0.98$ Å (d: spacing of lattice planes). In this 2θ range, most sharp profiles were observed with full-widths at half-maximum ranging from 0.008 to 0.019°. MEM analyses were performed using MEED[23] with the unit cell divided into 64 × 64 × 128 pixels and whole-pattern fitting using RIETAN-2000.[4,16] Electron-density images were drawn with the VEND program to visualize the 3D distribution of electrons and atomic nuclei.[24]

TOF Neutron Diffraction Experiments and Rietveld Refinement. TOF neutron powder diffraction data of $Sr_{9.3}Ni_{1.2}(PO_4)_7$ were collected at RT on the powder diffractometer Vega ($\Delta d/d \approx 2 \times 10^{-3}$) at the pulsed spallation neutron facility KENS. About 8.0 g of the sample was loaded into a V holder (diameter: 9.2 mm), which was slowly rotated during the measurement. An array of 160 position-sensitive detectors (PSDs) installed in a backward bank with a 2θ range from 150 to 170° was used to measure the intensity data. Incident neutron spectra were monitored with a ^{3}He monitor counter. Differences in efficiency between the PSDs and the monitor counter were corrected with intensity data taken in a separate measurement of incoherent scattering from V.

TOF neutron powder diffraction data in a d range from 0.55 to 5.0 Å were analyzed by the Rietveld method with RIETAN-2001T.[25] A composite background function (i.e., a 14th-order Legendre polynomial multiplied by a smoothed incident spectrum) was fit to the background. Bound coherent scattering lengths, b_c, used for the Rietveld refinement were 7.02 fm (Sr), 10.30 fm (Ni), 5.13 fm (P), and 5.803 fm (O).[26]

Physical Characterization. Second-harmonic-generation (SHG) responses of the powder samples were measured in a reflection mode. A Q-switch pulsed Nd:YAG laser operated at a wavelength of $\lambda_\omega = 1064$ nm was used as the radiation source with a repetition rate of 4 impulses/s and an impulse duration of about 12 ns. The laser beam was split into two beams to excite the radiation at the halved wavelength, $\lambda_{2\omega} = 532$ nm, simultaneously in samples to be measured and in a reference sample, polycrystalline α-SiO_2. The incident-beam peak power was about 0.1 MW on a spot 3 mm in diameter on the surface of the sample.

Magnetic susceptibilities, χ, of $Sr_{9.3}Ni_{1.2}(PO_4)_7$ were measured on a DC SQUID magnetometer (Quantum Design, MPMS) between 5 and 300 K in an applied field of 100 Oe (1 Oe = $[10^3/4\pi]$ A m^{-1}) under both zero-field-cooled (ZFC) and field-cooled (FC) conditions.

The infrared spectrum of $Sr_{9.3}Ni_{1.2}(PO_4)_7$ was measured on a Nicolet Magna-750 Fourier spectrometer in a wavenumber ($\tilde{\nu}$) range from 4000 to 400 cm^{-1} by the Nujol mull method.

Electron Microscopy Observations. $Sr_{9.3}Ni_{1.2}(PO_4)_7$ was deposited on holey carbon grids. Selected-area electron diffraction patterns were taken on a Philips CM20 electron microscope. Crystal-structure images were observed on a JEOL 4000 EX electron microscope having a Scherzer resolution limit of 1.7 Å and operated at 400 kV. Crystal-structure images were also simulated by the multislice method using the MacTempas program.

3. Results

3.1. Phase Formation in $Sr_{9+x}Ni_{1.5-x}(PO_4)_7$. The samples with nominal compositions of $Sr_{9+x}Ni_{1.5-x}(PO_4)_7$ ($x = 0.15-0.35$) were monophasic whereas those with $x = 0$ and 0.1 and those with $x = 0.4$, 0.45, and 0.5 contained $Sr_2Ni(PO_4)_2$ and $Sr_3(PO_4)_2$ concomitantly. Table 1 summarizes the lattice parameters and constituent phases of $Sr_{9+x}Ni_{1.5-x}(PO_4)_7$ ($0 \le x \le 0.5$). Figure 2 displays plots of lattice parameters against x. These experimental data show $Sr_{9+x}Ni_{1.5-x}(PO_4)_7$ to have a compositional range of $0.14 \le x \le 0.39$.

3.2. Physical Properties of $Sr_{9.3}Ni_{1.2}(PO_4)_7$. Figure 3 presents plots of χ^{-1} and χT against temperature, T, for $Sr_{9.3}Ni_{1.2}(PO_4)_7$. No noticeable difference was found between the curves measured under the ZFC and FC

(19) Toraya, H. *J. Appl. Crystallogr.* **1990**, *23*, 485.
(20) Dong, C. *J. Appl. Crystallogr.* **1999**, *32*, 838.
(21) *International Tables for Crystallography*, 2nd ed.; Kluwer: Dordrecht, The Netherlands, 1999; Vol. C, pp 572−574.
(22) Kissel, L.; Pratt, R. H. *Acta Crystallogr., Sect. A* **1990**, *46*, 170.
(23) Kumazawa, S.; Kubota, Y.; Takata, M.; Sakata, M.; Ishibashi, Y. *J. Appl. Crystallogr.* **1993**, *26*, 453.
(24) Dilanian, R. A.; Izumi, F. Unpublished work.
(25) Ohta, T.; Izumi, F.; Oikawa, K.; Kamiyama, T. *Physica B* **1997**, *234−236*, 1093.
(26) *International Tables for Crystallography*, 2nd ed.; Kluwer: Dordrecht, The Netherlands, 1999; Vol. C, pp 440−450.

Table 1. Lattice Parameters and Phase Compositions for $Sr_{9+x}Ni_{1.5-x}(PO_4)_7$ ($0 \le x \le 0.5$)

x	a/Å	c/Å	impurity (mass fraction)	composition of the main phase[a]
0	10.5840(5)	19.6811(8)	$Sr_2Ni(PO_4)_2$ (6.5%)	$Sr_{9.14}Ni_{1.36}(PO_4)_7$
0.1	10.5836(5)	19.6789(8)	$Sr_2Ni(PO_4)_2$ (1.8%)	$Sr_{9.14}Ni_{1.36}(PO_4)_7$
0.15	10.5844(5)	19.6797(8)		$Sr_{9.15}Ni_{1.35}(PO_4)_7$
0.2	10.5930(5)	19.6733(8)		$Sr_{9.20}Ni_{1.30}(PO_4)_7$
0.25	10.6000(5)	19.6651(8)		$Sr_{9.25}Ni_{1.25}(PO_4)_7$
0.3	10.6070(5)	19.6584(8)		$Sr_{9.30}Ni_{1.20}(PO_4)_7$
0.35	10.6170(5)	19.6472(8)		$Sr_{9.35}Ni_{1.15}(PO_4)_7$
0.4	10.6229(5)	19.6414(8)	$Sr_3(PO_4)_2$ (0.6%)	$Sr_{9.39}Ni_{1.11}(PO_4)_7$
0.45	10.6222(5)	19.6422(8)	$Sr_3(PO_4)_2$ (4.8%)	$Sr_{9.40}Ni_{1.10}(PO_4)_7$
0.5	10.6233(5)	19.6410(8)	$Sr_3(PO_4)_2$ (10.3%)	$Sr_{9.39}Ni_{1.11}(PO_4)_7$

[a] Compositions of $Sr_{9+x}Ni_{1.5-x}(PO_4)_7$ were calculated from the mass fractions of the impurities.

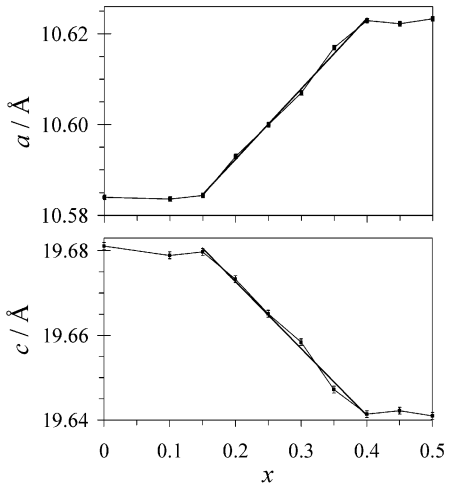

Figure 2. Lattice parameters of $Sr_{9+x}Ni_{1.5-x}(PO_4)_7$ ($0 \le x \le 0.5$) plotted against x.

conditions. The χ^{-1} versus T curve obeyed the Curie–Weiss equation over the whole temperature range, 5–300 K:

$$\chi^{-1} = (T - \theta)/C \qquad (1)$$

where θ (= −4.66 K) is the Weiss constant and C (= 1.61 emu K mol^{-1}) is the Curie constant. $Sr_{9.3}Ni_{1.2}(PO_4)_7$ is therefore paramagnetic over the whole temperature range. The effective magnetic moment, $\mu_e = (8C)^{1/2}$, was calculated at $3.28\mu_B$ (μ_B: Bohr magneton) per Ni^{2+} ion. This value is larger than the theoretical value, $2.83\mu_B$, that was expected for the free Ni^{2+} ion.[27] Such a difference between the experimental and theoretical magnetic moments is ascribable to the contribution of the spin–orbital interaction and is sometimes observed in compounds containing Ni^{2+} ions.[27]

The infrared spectrum of $Sr_{9.3}Ni_{1.2}(PO_4)_7$ was similar to that of an isotypic phosphate, $Sr_9Fe_{1.5}(PO_4)_7$.[12] Absorption bands due to P–O stretching and O–P–O bending vibrations appeared in $\tilde{\nu}$ ranges of 1400–800 and 650–500 cm^{-1}, respectively.

No SHG response was detected, which offers evidence that $Sr_{9.3}Ni_{1.2}(PO_4)_7$ has a center of symmetry.

3.3. Structure Analysis of $Sr_{9.3}Ni_{1.2}(PO_4)_7$. 3.3.1. Electron Diffraction. Figure 4 shows selected-area electron diffraction patterns taken for $Sr_{9.3}Ni_{1.2}(PO_4)_7$ along four different directions. Spots in the patterns could be indexed in a trigonal system with lattice parameters of $a \approx 10.6$ Å and $c \approx 19.7$ Å (hexagonal axes). The $[11\bar{2}0]^*$ diffraction pattern exhibits a rhombohedral shift of the spot rows along $\boldsymbol{c}^*$ by $hc^*/3$. Reflection conditions of $-h + k + l = 3n$ for $hkil$, $h + l = 3n$ for $h\bar{h}0l$, and $l = 3n$ for $hh\overline{2h}l$ (hexagonal axes, obverse setting)[28] afford the possible space groups $R3$, $R\bar{3}$, $R32$, $R3m$, and $R\bar{3}m$. Accordingly, $Sr_{9.3}Ni_{1.2}(PO_4)_7$ belongs to either $R\bar{3}$ or $R\bar{3}m$, considering that space groups $R3$, $R32$, and $R3m$ are noncentrosymmetric.

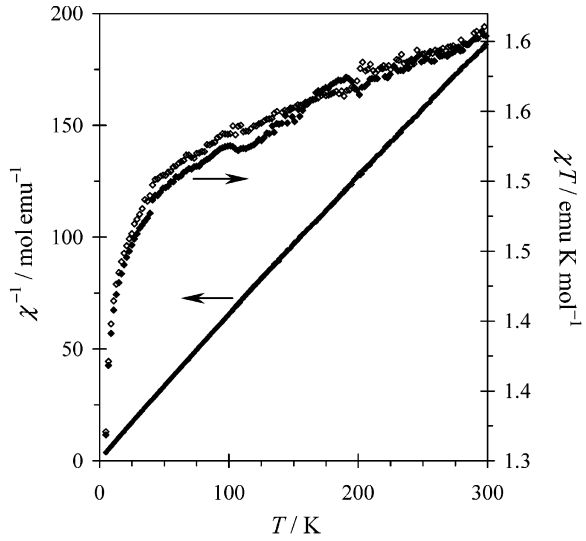

Figure 3. Inverse magnetic susceptibilities, χ^{-1}, and χT plotted against temperature for $Sr_{9.3}Ni_{1.2}(PO_4)_7$ with the zero-field-cooling (◆) and field-cooling modes (◇) in an applied field of 100 Oe.

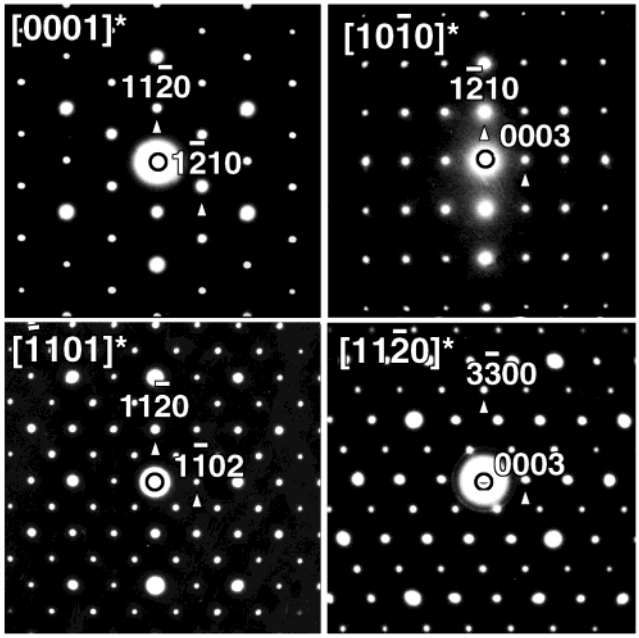

Figure 4. Selected-area electron diffraction patterns taken along the [0001]*, [10$\bar{1}$0]*, [$\bar{1}$101]*, and [11$\bar{2}$0]* zone axes for $Sr_{9.3}Ni_{1.2}(PO_4)_7$.

(27) Kittel, C. *Introduction to Solid State Physics*, 6th ed.; Wiley & Sons: New York, 1986, p 406.
(28) *International Tables for Crystallography*, 5th ed.; Kluwer: Dordrecht, The Netherlands, 2002; Vol. A, p 52.

3.3.2. Structure Refinement from the Synchrotron XRD Data. Structure parameters of $Sr_{9.3}Ni_{1.2}(PO_4)_7$ were refined by assuming space group $R\bar{3}m$ (no. 166), which has higher symmetry than $R\bar{3}$. Fractional coordinates in β-$Ca_3(PO_4)_2$[29] with space group $R3c$ ($Z = 21$; $a = 10.439$ Å and $c = 37.375$ Å) were converted into those in $Sr_{9.3}Ni_{1.2}(PO_4)_7$ according to a cell transformation: $\boldsymbol{a}' = -\boldsymbol{a}$, $\boldsymbol{b}' = -\boldsymbol{b}$, and $2\boldsymbol{c}' = \boldsymbol{c}$.[12,13] The resulting fractional coordinates were used as initial parameters for Rietveld refinement. From now on, site names similar to those for $Sr_9Fe_{1.5}(PO_4)_7$[12] will be given for $Sr_{9.3}Ni_{1.2}(PO_4)_7$.

In the initial structural model of $Sr_{9.3}Ni_{1.2}(PO_4)_7$, Sr, Ni, and P atoms were located at Sr1 (18*h*; $x \approx 0.190$ and $z \approx 0.537$), Sr3 (9*e*), M4 (6*c*; $z \approx 0.354$) with occupancies, *g*, of $g(\mathrm{Sr}) = 0.15$ and $g(\mathrm{Ni}) = 0.1$, Ni5 (3*a*), P1 (3*b*), and P2 (18*h*; $x \approx 0.493$ and $z \approx 0.397$). The O atoms bonded to the P1 atom at an inversion center were O11 (18*h*; $x \approx 0.93$ and $z \approx 0.54$) and O12 (6*c*; $z \approx 0.578$) with $g(\mathrm{O11}) = g(\mathrm{O12}) = {}^1/_2$. The P2 site was surrounded by O21 (18*h*; $x \approx 0.535$ and $z \approx 0.677$), O22 (36*i*; $x \approx 0.266$, $y \approx 0.013$, and $z \approx 0.235$), and O24 (18*h*; $x \approx 0.911$ and $z \approx 0.067$) sites that were filled completely.

The subsequent Rietveld refinement afforded extraordinally large *U* parameters for the Sr3, O11, and O12 sites: $U(\mathrm{Sr3}) = 9.1(10)$ nm^2, $U(\mathrm{O11}) = 6.5(5)$ nm^2, and $U(\mathrm{O12}) = 96(14)$ nm^2. These findings prompted us to build a split-atom model: model I. In model I, the Sr3 atom was shifted from site 9*e* to site 18*h* ($x \approx 0.479$ and $z \approx 0.0094$) with $g(\mathrm{Sr3}) = {}^1/_2$, and the oxygen atoms involved in the $P1O_4$ tetrahedron were located at a general position O11 (36*i*; $x \approx 0.96$, $y \approx 0.10$, and $z \approx 0.54$) with $g(\mathrm{O11}) = {}^1/_3$.

Model I yielded the following *R* factors and *U* parameters: $R_{wp} = 7.13\%$ ($S = R_{wp}/R_e = 3.02$), $R_p = 5.13\%$, $R_B = 3.88\%$, and $R_F = 2.95\%$; $U(\mathrm{Sr1}) = 0.931(14)$ nm^2, $U(\mathrm{Sr3}) = 2.22(3)$ nm^2, $U(\mathrm{M4}) = 2.95(12)$ nm^2, $U(\mathrm{Ni5}) = 0.51(4)$ nm^2, $U(\mathrm{P1}) = 3.72(11)$ nm^2, $U(\mathrm{P2}) = 0.62(3)$ nm^2, $U(\mathrm{O11}) = 5.5(3)$ nm^2, $U(\mathrm{O21}) = 1.97(9)$ nm^2, $U(\mathrm{O22}) = 1.29(6)$ nm^2, and $U(\mathrm{O24}) = 0.59(8)$ nm^2. The *U* parameters of the Sr3, M4, P1, and O11 sites were still unusually large because of the split-atom model that is far from perfect, which urged us to modify model I further.

We expected MPF to enable us to extract structural details that had not been introduced into the above preliminary structural model. Then, we determined the electron-density distribution in $Sr_{9.3}Ni_{1.2}(PO_4)_7$ by the MPF method from F_o(Rietveld) data estimated after the Rietveld refinement by adopting model I. After two REMEDY cycles, R_{wp} (*S*), R_p, R_B, and R_F dropped to 6.60 (2.80), 4.62, 1.31, and 1.01%, respectively. The dramatic improvements in R_B and R_F calculated from the $|F_o(\mathrm{Rietveld})|$ data show that the complicated disordered structure of $Sr_{9.3}Ni_{1.2}(PO_4)_7$ is represented more adequately with electron densities than with structure parameters based on model I.

Figure 5a displays an electron-density image in a *z* range of $0.64 \le z \le 0.73$, where Sr3, M4, Ni5, P2, O21, and O24 atoms are included, and Figure 6a illustrates an electron-density image for the $P1O_4$ tetrahedron. The dotted arrows in these Figures denote splitting of the Sr3, M4, and O11 atoms. A close examination of these images allowed us to modify model I to build a better

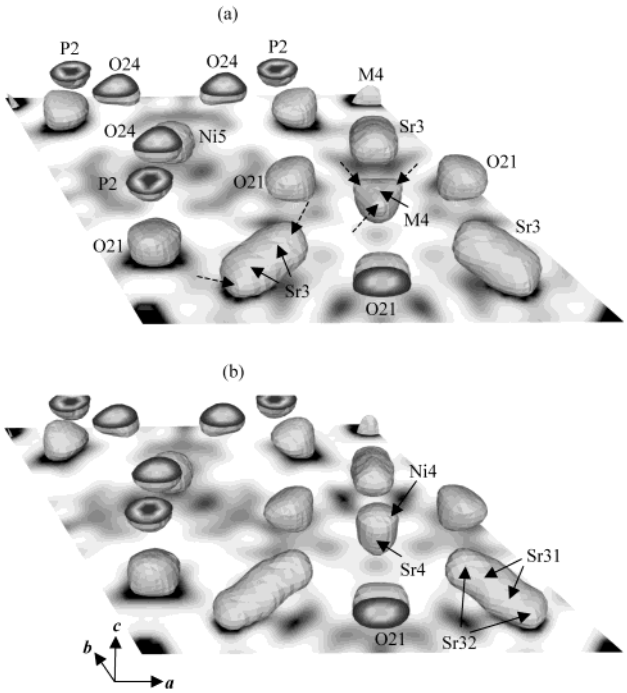

Figure 5. Electron-density distribution determined by MPF with (a) model I and (b) model II in the region of $0.64 \le z \le 0.73$. Isosurfaces for an equidensity level of 2 e Å^{-3} and the section at $z = 0.64$ were drawn with VEND.[24] Dotted arrows in (a) indicate the splitting of the Sr3 and M4 atoms.

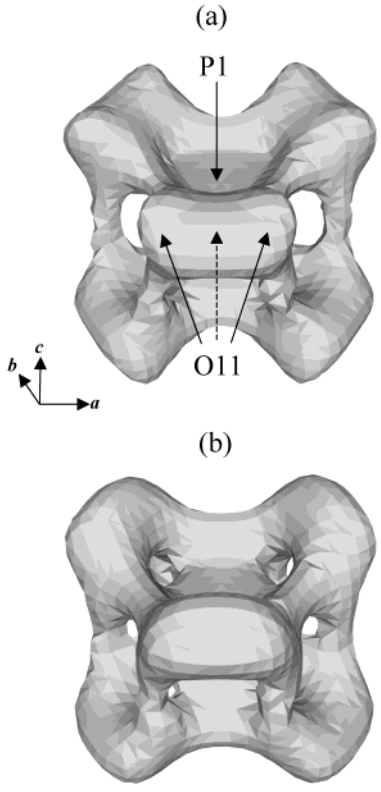

Figure 6. Electron-density distribution determined for the $P1O_4$ tetrahedron by MPF with (a) model I and (b) model II. Isosurfaces for an equidensity level of 1.2 e Å^{-3} were drawn with VEND.[24] Dotted arrows in (a) indicate the splitting of O atoms bonded to the P1 site.

(29) Dickens, B.; Schroeder, L. W.; Brown, W. E. *J. Solid State Chem.* **1974**, *10*, 232.

Table 2. Conditions of the Diffraction Experiments and Parts of the Refinement Results for $Sr_{9.3}Ni_{1.2}(PO_4)_7$

beam	synchrotron XRD	TOF neutron
λ/Å	0.8000	
d range/Å	0.983−8.818	0.55−5.0
2θ range/deg	5.2−48.0	
number of data points	14268	3845
temperature/K	100	295
lattice parameters:		
a/Å	10.59280(1)	10.60940(13)
c/Å	19.63191(2)	19.6678(2)
V/Å^3	1907.720(4)	1917.20(4)
number of Bragg reflections	287	1501
number of variables:		
background/profiles	12/10	15/18
structure/lattice	36/2	55/2
others	2	2
R_{wp}; R_p	5.39%; 3.93%	3.20%; 2.65%
R_B; R_F	2.80%; 1.88%	1.65%; 1.83%
S	2.30	1.48

split-atom model for Rietveld analysis: model II. MPF can be distinguished from Fourier/D synthesis by the ease with which additional sites can be detected in electron-density maps because of high S/N ratios and the absence of negative electron densities.[4,16] If the structural model were modified by trial and error in the absence of the electron-density images, no details in such disordered atomic arrangements could be deduced even from our synchrotron XRD data taken with an instrumental resolution at the top international level.

In model II, each Sr3 atom was split into four fractions: Sr31 (18*h*; $x \approx 0.486$ and $z \approx 0.008$) and Sr32 (18*h*; $x \approx 0.460$ and $z \approx 0.014$). U(Sr31) and U(Sr32) were constrained to be equal to each other. Sr^{2+} ions were distributed between the Sr31 and Sr32 sites such that g(Sr31) + g(Sr32) = $^1/_2$. Sr^{2+} and Ni^{2+} ions at the M4 site were split into several pieces. Sr^{2+} ions were retained at site 6*c* ($z \approx 0.348$; Sr4) with g(Sr4) = 0.15 whereas Ni^{2+} ions were displaced from the ideal 6*c* site to an 18*h* site ($x \approx 0.007$ and $z \approx 0.371$; Ni4) that is slightly off the 3-fold rotational axis with g(Ni4) = $^1/_{30}$. U(Sr4) and U(Ni4) were constrained to be equal to each other.

The P1 atom was displaced from site 3*b* to site 18*h* ($x \approx 0.014$ and $z \approx 0.504$) with g(P1) = $^1/_6$, in view of the large U(P1) parameter in model I. Fractional coordinates (x and z) and a U parameter for the P1 atom were refined in turn (in different cycles of Rietveld analysis) because they were strongly correlated with each other. The O atoms arranged tetrahedrally around the P1 atom were located at an 18*h* site ($x \approx 0.924$ and $z \approx 0.550$; O11) and a 36*i* site ($x \approx 0.002$, $y \approx 0.120$, and $z \approx 0.534$; O12) with U(O11) and U(O12) constrained to be equal to each other. A linear constraint, g(O11)/2 + g(O12) = $^1/_3$, was imposed on their occupancies.

The Rietveld refinement with model II gave R_{wp} = 5.39% (S = 2.30), R_p = 3.93%, R_B = 2.80%, and R_F = 1.88%, which are much lower than the R factors for model I. U parameters refined with model II for the disordered atoms, U(Sr31) = U(Sr32) = 0.75(3) nm^2, U(Sr4) = U(Ni4) = 1.5(3) nm^2, U(P1) = 1.25(9) nm^2, and U(O11) = U(O12) = 2.5(2) nm^2, were comparable to those for the ordered atoms. Table 2 lists the experimental and refinement conditions, lattice parameters, R factors, and so forth. Fractional coordinates and U parameters for the final Rietveld analysis appear in Table 3. Numbers in parentheses are estimated standard deviations of the last significant digits throughout this paper.

Finally, we carried out the structure refinement of $Sr_{9.3}Ni_{1.2}(PO_4)_7$ by MPF, which was started by analyzing F_o(Rietveld) data estimated after the Rietveld refinement by adopting model II. Two REMEDY cycles decreased R_{wp} (S), R_p, R_B, and R_F a great deal to 5.18 (2.20), 3.71, 1.03, and 0.82%, respectively. Subtle changes in electron densities arose out of MPF, which improved F_o(MPF) data and, in turn, the R factors. The striking decreases in R_B and R_F evaluated from observed integrated intensities are particularly noteworthy. Observed, calculated, and difference synchrotron XRD patterns for final MPF are plotted in Figure 7.

Figures 5b and 6b demonstrate the electron-density distribution in the same regions as with Figures 5a and 6a. Appreciable differences between Figure 5a and b and those between Figure 6a and b evidently arise from the improvement of the split-atom model and the estimation of the more accurate F_o(Rietveld) values in the Rietveld analysis based on model II.

3.3.3. Structure Refinement from the TOF Neutron Diffraction Data. Neutron diffraction is suitable for refining structure parameters of disordered atoms without any influences of inner-shell and valence electrons. For this reason, we also analyzed the TOF neutron powder diffraction data on the basis of model II. In the beginning, thermal vibrations of all the atoms were regarded as isotropic. At the final stage of the Rietveld analysis, we refined anisotropic atomic displacement parameters, U_{ij}, for the fully occupied sites—Sr1, Ni5, P2, O21, O22, and O24— which yielded rather low R factors: R_{wp} = 3.20% (S = 1.48), R_p = 2.65%, R_B = 1.65%, and R_F = 1.83%. Refining the occupancies of the ordered Sr1 and Ni5 sites (simultaneously with U_{ij}'s) resulted in a convergence to unity within the estimated standard deviations: g(Sr1) = 1.003(3) and g(Ni5) = 1.001(5).

Table 2 gives experimental and refinement conditions, lattice parameters, R factors, and so forth. Final fractional coordinates and $U(U_{eq})$ parameters for $Sr_{9.3}Ni_{1.2}(PO_4)_7$ are listed in Table 4, and U_{ij} parameters, in Table 5. Figure 8 displays observed, calculated, and difference TOF neutron-diffraction patterns for $Sr_{9.3}Ni_{1.2}(PO_4)_7$.

The Rietveld refinements of the synchrotron X-ray and TOF neutron powder diffraction data afforded comparable g(O11) and g(O12) values. However, g(Sr31) and g(Sr32) somewhat differed from each other between the two Rietveld refinements, which is ascribed to the difficulty in refining the occupancies of split sites because of high correlations with U parameters and fractional coordinates. The O21 site had the largest U parameter of the three fully occupied O sites for both the X-ray and TOF neutron-diffraction data, which will be discussed later.

3.3.4. Transmission Electron Microscopy. Crystal-structure images were taken along the [0001] and [10$\bar{1}$0] directions to see columns comprising metal and oxygen atoms (Figure 9). Brighter dots correspond to the columns of Ni atoms, and less-bright dots, to those of Sr atoms. Images simulated from the structure parameters listed in Table 4 for different defocus values, Δf,

Table 3. Structure Parameters of $Sr_{9.3}Ni_{1.2}(PO_4)_7$ Determined from the Synchrotron XRD Data

atom	site	*g*	*x*	*y*	*z*	U/nm^2
Sr1	18*h*	1	0.19009(2)	$=-x$	0.53723(2)	0.830(12)
Sr31	18*h*	0.344(8)	−0.5142(5)	$=-x$	0.00826(11)	0.75(3)
Sr32	18*h*	0.156[a]	−0.5405(7)	$=-x$	0.0139(3)	$=U$(Sr31)
Sr4	6*c*	0.15	0	0	0.3478(3)	1.5(3)
Ni4	18*h*	$^1/_{30}$	0.007(3)	$=-x$	0.3709(7)	$=U$(Sr4)
Ni5	3*a*	1	0	0	0	0.42(3)
P1	18*h*	$^1/_6$	0.0136(3)	$=-x$	0.5036(8)	1.25(9)
P2	18*h*	1	0.49268(5)	$=-x$	0.39668(6)	0.84(3)
O11	18*h*	0.343(11)	−0.5908(6)	$=-x$	0.1163(5)	2.5(2)
O12	36*i*	0.162[b]	0.2153(12)	0.5466(14)	0.1332(6)	$=U$(O11)
O21	18*h*	1	0.53513(11)	$=-x$	0.67704(11)	1.89(7)
O22	36*i*	1	0.26633(15)	0.01301(14)	0.23511(8)	1.34(5)
O24	18*h*	1	0.91102(9)	$=-x$	0.06717(10)	0.45(6)

[a] $g(\mathrm{Sr32}) = {}^1/_2 - g(\mathrm{Sr31})$. [b] $g(\mathrm{O12}) = {}^1/_3 - g(\mathrm{O11})/2$.

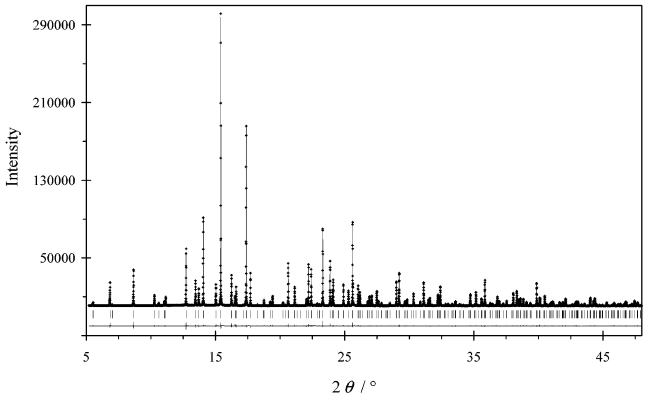

Figure 7. Observed (+), calculated (—), and difference patterns obtained by the final MPF structure refinement from the synchrotron XRD data for $Sr_{9.3}Ni_{1.2}(PO_4)_7$. Tick marks denote the peak positions of possible Bragg reflections.

and thicknesses, *t*, agreed well with those of different parts in the observed images. The inset of Figure 9 gives a crystal-structure image calculated with $\Delta f = -80$ nm and $t = 33$ nm for the $[10\bar{1}0]$ zone.

4. Discussion

All the reflections in the electron diffraction patterns and the synchrotron X-ray and TOF neutron powder diffraction patterns of $Sr_{9.3}Ni_{1.2}(PO_4)_7$ were indexed on the basis of the trigonal system (space group $R\bar{3}m$) and lattice parameters of $a \approx 10.6$ Å and $c \approx 19.7$ Å. As described previously, the crystallinity of this compound was high enough to give rise to the sharp reflection profiles. Neither split spots nor streaks were seen in the electron diffraction patterns (Figure 4). The observed crystal-structure images coincided well with the simulated ones. All of these facts concerning the structure of $Sr_{9.3}Ni_{1.2}(PO_4)_7$ support our structural model where the Sr3 and M4 atoms and the $P1O_4$ tetrahedra are statistically disordered without forming a superstructure or an appreciable number of defects. Sr1 and Ni5 atoms and $P2O_4$ tetrahedra are seated in definite positions without suffering noticeable influences from the other disordered atoms.

Using MPF followed by 3D visualization of electron densities, we could build the expedient split-atom model II that describes the highly disordered structure of $Sr_{9.3}Ni_{1.2}(PO_4)_7$ much better than model I. The improvement in the structural model is responsible for the lower *R* factors and the more-reasonable *U* parameters of the disordered atoms in model II than those in model I. The notable decreases in the *R* factors by the final MPF structure refinement demonstrate that the positional and orientational disorder in $Sr_{9.3}Ni_{1.2}(PO_4)_7$ is still better expressed with electron densities than with the structure parameters in conventional Rietveld analysis. Structural representation taking into account bonding electrons in predominantly covalent P—O bonds will also contribute to the improvements in the *R* factors.

The Sr1 and Ni5 sites are fully occupied. The short Ni5—O bond length of 2.099 Å excludes the possibility for Sr^{2+} ions to occupy the Ni5 site. In addition, the refinement of *g*(Sr1) and *g*(Ni5) from the TOF neutron-diffraction data provides unambiguous evidence for full occupation of these two sites. The Sr3 atoms are randomly distributed among the four positions with the total occupation probability of unity. The two separate sites were assigned to Sr^{2+} and Ni^{2+} ions occupying the positions corresponding to the M4 site in the β-$Ca_3(PO_4)_2$-type structure.[29] Such relative shifts of Sr4 and Ni4 are explained in terms of the large difference between the effective ionic radii, *r*,[30] of Ni^{2+} ($r = 0.69$ Å for 6-fold coordination) and Sr^{2+} ($r = 1.18$ Å) ions. Model II afforded reasonable Sr4—O interatomic distances, *l*: *l*(Sr4—O11) = 2.435(11) Å (×3), *l*(Sr4—O12) = 2.649(14) Å (×6), and *l*(Sr4—O21) = 2.415(2) Å (×3). Locating Ni^{2+} ions at the M4 site also yielded acceptable bond lengths for Ni^{2+} ions: *l*(Ni4—O11) = 1.99(5) and 2.13(2) Å (×2), *l*(Ni4—O12) = 2.20(4) (×2), 2.26(2) (×2), and 2.33(3) Å (×2), and *l*(Ni4—O21) = 2.41(3) Å (×2).

The M4 (6*c*; $z \approx 0.354$) site is unfavorable for small M^{2+} ions such as Fe^{2+}, Ni^{2+}, and Cu^{2+} owing to the large average *l*(M4—O) value of ca. 2.4 Å. Nevertheless, all the solid solutions of $Sr_{9+x}M_{1.5-x}(PO_4)_7$ (M = Mn, Fe, Co, Ni, Cu, and Cd) occur in a compositional range of $x < 0.40$;[12] in other words, the M4 site is occupied not only by Sr^{2+} ions but also M^{2+} ions. In $Sr_{9+x}Ni_{1.5-x}(PO_4)_7$ with $0.14 \le x \le 0.39$, *g*(Sr4) should range from 0.07 to 0.195 on the assumption that the Sr1, Sr3, and Ni5 sites are completely filled. In solid solutions of $Sr_{9+x}M_{1.5-x}(PO_4)_7$ (M = Mg, Zn, and Cd), the boundary of the M-rich side was found to lie at $x = -2.28$ for M = Mg,[31] $x = -1.34$ for M = Zn,[31] and $x = -0.71$ for M = Cd.[32] Mg^{2+}, Zn^{2+}, and Cd^{2+} ions must therefore occupy sites corresponding to Sr1 or Sr3 if $x < 0$.

(30) Shannon, R. D. *Acta Crystallogr., Sect. A* **1976**, *32*, 751.
(31) Sarver, J. F.; Hoffman, M. V.; Hummel, F. A. *J. Electrochem. Soc.* **1961**, *108*, 1103.
(32) Looney, J. R.; Brown, J. J. *J. Electrochem. Soc.* **1971**, *118*, 470.

Table 4. Structure Parameters of $Sr_{9.3}Ni_{1.2}(PO_4)_7$ Determined from the TOF Neutron Diffraction Data

atom	site	g	x	y	z	U or U_{eq}/nm^2
Sr1	18*h*	1	0.19024(8)	$= -x$	0.53719(7)	0.89[a]
Sr31	18*h*	0.300(11)	−0.5120(7)	$= -x$	0.0068(5)	0.82(11)
Sr32	18*h*	0.200[b]	−0.5382(8)	$= -x$	0.0150(5)	$= U$(Sr31)
Sr4	6*c*	0.15	0	0	0.3499(8)	0.2(5)
Ni4	18*h*	$^1/_{30}$	0.010(3)	$= -x$	0.3716(11)	$= U$(Sr4)
Ni5	3*a*	1	0	0	0	0.56[a]
P1	18*h*	$^1/_6$	0.0129(13)	$= -x$	0.5096(9)	0.7(6)
P2	18*h*	1	0.49277(11)	$= -x$	0.39674(11)	0.91[a]
O11	18*h*	0.342(10)	−0.5917(5)	$= -x$	0.1176(4)	3.6(2)
O12	36*i*	0.162[c]	0.2146(11)	0.5456(11)	0.1335(5)	$= U$(O11)
O21	18*h*	1	0.53448(9)	$= -x$	0.67653(10)	2.72[a]
O22	36*i*	1	0.26592(13)	0.01286(12)	0.23450(6)	1.32[a]
O24	18*h*	1	0.91104(9)	$= -x$	0.06737(9)	0.90[a]

[a] Equivalent isotropic atomic-displacement parameter defined as $U_{eq} = (^1/_3)\sum_i\sum_j U_{ij}a^*_i a^*_j \boldsymbol{a}_i \boldsymbol{a}_j$. [b] g(Sr32) = $^1/_2 - g$(Sr31). [c] g(O12) = $^1/_3 - g$(O11)/2.

Table 5. Anisotropic Atomic-Displacement Parameters[a] (nm^2) for the Fully Occupied Sites in $Sr_{9.3}Ni_{1.2}(PO_4)_7$

atom	U_{11}	U_{22}	U_{33}	U_{12}	U_{13}	U_{23}
Sr1	0.69(6)	$= U_{11}$	0.55(9)	−0.22(7)	−0.02(3)	$= -U_{13}$
Ni5	0.57(10)	$= U_{11}$	0.55(14)	$= U_{11}/2$	0	0
P2	1.25(9)	$= U_{11}$	0.64(12)	0.93(11)	−0.05(5)	$= -U_{13}$
O21	4.49(12)	$= U_{11}$	0.34(12)	3.11(13)	−0.40(6)	$= -U_{13}$
O22	0.94(8)	0.54(7)	1.61(9)	−0.28(7)	−0.31(7)	−0.49(6)
O24	0.57(8)	$= U_{11}$	1.35(12)	0.14(9)	0.04(4)	$= -U_{13}$

[a] The anisotropic Debye−Waller factor is computed as $\exp[-2\pi^2(h^2a^{*2}U_{11} + k^2b^{*2}U_{22} + l^2c^{*2}U_{33} + 2hka^*b^*U_{12} + 2hla^*c^*U_{13} + 2klb^*c^*U_{23})]$.

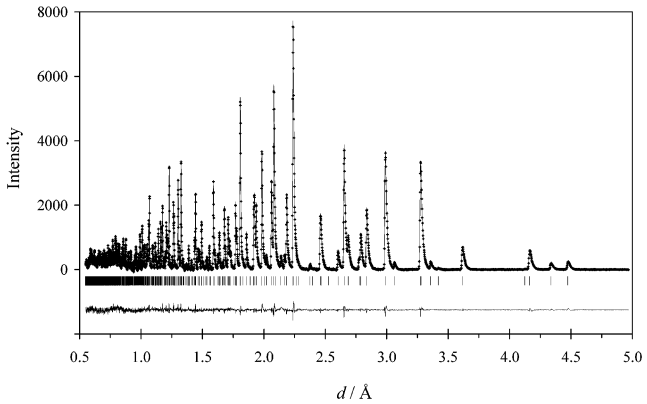

Figure 8. Observed (+), calculated (—), and difference patterns resulting from the Rietveld analysis of the TOF neutron powder diffraction data for $Sr_{9.3}Ni_{1.2}(PO_4)_7$. Tick marks denote the peak positions of possible Bragg reflections. Background intensities were subtracted from the observed and calculated intensities.

The Sr3 and M4 atoms form an infinite 2D network perpendicular to the *c* axis (Figure 5). The M4 site is 75% vacant, and the Sr3 and M4 atoms are highly disordered with effective interatomic distances of l(Sr31−Sr31) = 0.61 Å, l(Sr31−Sr32) = 0.50 Å, l(Sr32−Sr32) = 1.58 Å, and l(Sr32−Sr4) = 2.32 Å. Hence, high ionic conductivity is expected on the [001] plane.

The $P1O_4$ tetrahedron is orientationally disordered. The disordering of the four O atoms covalently bonded to the P1 atom is rather complex, as can be appreciated from Figure 6. The split-atom models are incapable of describing such pronounced orientational disorder adequately. The disordered arrangements of O11 and O12 must be partly absorbed into the U(O11) and U(O12) parameters to make them unusually large in both Rietveld refinements with the synchrotron X-ray and TOF neutron-diffraction data.

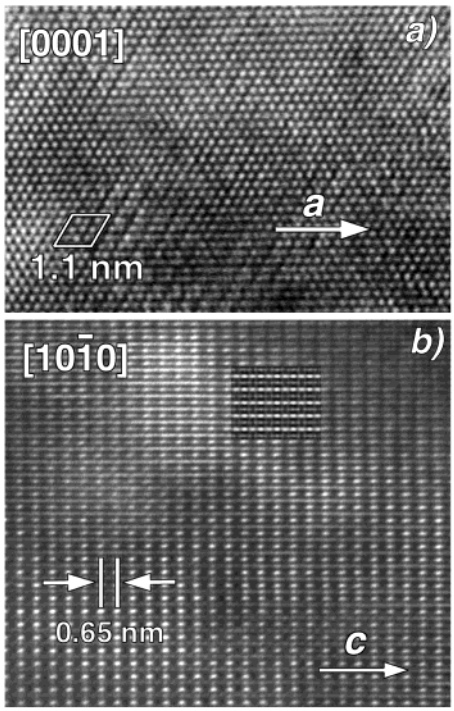

Figure 9. Crystal-structure images of $Sr_{9.3}Ni_{1.2}(PO_4)_7$ taken along the (a) [0001] and (b) [10$\bar{1}$0] zones. The inset gives an image calculated for the [10$\bar{1}$0] zone with $\Delta f = -80$ nm and $t = 33$ nm.

Some atoms with $g = 1$ owe their apparently anisotropic thermal motion (Table 5) to the bonds between them and the disordered atoms. The thermal ellipsoid of the Sr1 atom is elongated along the [1$\bar{1}$0] direction whereas that of the P2 atom is perpendicular to this direction. Thermal vibrations of the O21 and O22 atoms appeared to be very anisotropic along directions perpendicular to the P−O bonds. The MPF method afforded an electron-density distribution in accord with the seemingly anisotropic thermal motion. For example, a sectional view of electron densities for the O21 atom exhibited ellipsoidal distribution. Because the O21 atom is bonded to the highly disordered Sr31, Sr32, Sr4, and Ni4 atoms, it is unnecessarily disordered to some extent as well. Such static positional disorder is readily absorbed into the U_{ij} parameters.

In the present investigation, MPF has enabled us to gain a better understanding of the highly disordered atomic arrangements in $Sr_{9.3}Ni_{1.2}(PO_4)_7$. In MPF, the

repartition of observed diffraction intensities is rapidly improved during REDEMY cycles thanks to the introduction of F_c(MEM) into whole-pattern fitting. Hence, the MPF method is superior to the MEM/Rietveld method,[1] where the analytical method in the Fourier synthesis of F_o(Rietveld) data is merely replaced with MEM. From the results acquired in this work, we conclude MPF to be a very powerful method of structure refinement in which imperfect structural representations in conventional Rietveld analysis are supplemented with model-free MEM. We will further apply MPF to a variety of compounds with complicated disordered structures in order to clarify their structural properties.

Acknowledgment. This work was partially supported by the Russian Foundation for Basic Research (grants 00-03-32660, 01-03-06121, and 01-03-06122). We thank the staff of beam line BL15XU at SPring-8 for technical assistance. A.A.B. acknowledges the award of the STA Fellowship from the Japan Science and Technology Corporation. V.A.M. is grateful to DWTC and IUAP V-1 (Belgium) for financial support.

CM0206901